AGU PUBLICATIONS

Space Weather

RESEARCH ARTICLE
10.1002/2013SW001012

Key Points:
- First time auroral ionospheric Ti prediction
- Predictions of Ti demonstrated out to 81 days
- Demonstration that CIRs are geoeffective in ionosphere on a case by case basis

Correspondence to:
J. J. Sojka,
jan.sojka@usu.edu

Citation:
Sojka, J. J., R. W. Schunk, and M. J. Nicolls (2014), Ionospheric ion temperature forecasting in multiples of 27 days, *Space Weather*, *12*, 148–160, doi:10.1002/2013SW001012.

Received 8 NOV 2013
Accepted 26 FEB 2014
Accepted article online 3 MAR 2014
Published online 19 MAR 2014

Ionospheric ion temperature forecasting in multiples of 27 days

Jan J. Sojka[1], Robert W. Schunk[1], and Michael J. Nicolls[2]

[1]Center for Atmospheric and Space Sciences, Utah State University, Logan, Utah, USA, [2]SRI International, Menlo Park, California, USA

Abstract The ionospheric variability found at auroral locations is usually assumed to be unpredictable. The magnetosphere, which drives this ionospheric variability via storms and substorms, is at best only qualitatively describable. In this study we demonstrate that over a 3 year period, ionospheric variability observed from Poker Flat, Alaska, has, in fact, a high degree of long-term predictability. The observations used in this study are (a) the solar wind high speed stream velocity measured by the NASA Advanced Composition Explorer satellite, used to define the corotating interaction region (CIR), and (b) the ion temperature at 300 km altitude measured by the National Science Foundation Poker Flat Incoherent Scatter Radar over Poker Flat, Alaska. After determining a seasonal and diurnal climatology for the ion temperature, we show that the residual ion temperature heating events occur synchronously with CIR-geospace interactions. Furthermore, we demonstrate examples of ion temperature forecasting at 27, 54, and 81 days. A rudimentary operational forecasting scenario is described for forecasting recurrence 27 days ahead for the CIR-generated geomagnetic storms. These forecasts apply specifically to satellite tracking operations (thermospheric drag) and emergency HF-radio communications (ionospheric modifications) in the polar regions. The forecast is based on present-day solar and solar wind observations that can be used to uniquely identify the coronal hole and its CIR. From this CIR epoch, a 27 day forecast is then made.

1. Introduction

This paper demonstrates a new approach to forecasting a specific contribution to ionospheric weather many weeks into the future based on the current ionospheric condition. The present-day approaches to ionospheric forecasting are based on modeling either ionospheric climatology or storm-type weather based on observations of solar/solar wind disturbances driving physical models of the ionosphere. Ionospheric climatology has well-defined cycles, including solar, seasonal, and diurnal. These span time scales of years, weeks, and hours. A commonly used model that contains this ionospheric information is the International Reference Ionosphere (IRI) [*Bilitza*, 2001]. The IRI is an empirical model of the global ionosphere based on a wide variety of measurements covering different regions both from the ground and space and spanning many decades. Hence, this model has a coefficient database designed to capture typical (or average/median) ionospheric conditions as a function of location, solar cycle, season, and local time. More recently, the IRI has been augmented with a hybrid ionospheric storm capability based on both observations and ionosphere-thermosphere modeling [*Araujo-Pradere et al.*, 2004]. The use of the IRI or other empirical models can provide long-term forecasting of the median ionospheric state. The other major approach to ionospheric forecasting is to study and model the physical processes that drive and modify the ionosphere [*Schunk et al.*, 2005].

Our understanding of space weather is primarily based on the following paradigm: weather on the Sun initiates a sequence of events that propagate through the solar wind, the magnetosphere, and ultimately into the ionosphere and thermosphere. The prediction of severe space weather events involves forecasting the Sun-solar wind-magnetosphere system such that the ionospheric drivers can be determined. A prediction can then be made by running a physics-based ionospheric model driven by these storm inputs. At present, the forecast capability of this first step is less than 2 days and more typically only hours [*Sojka et al.*, 1998, *Schunk et al.*, 2005]. The most comprehensive modeling work involves developing coupled models of each region from the Sun to the ionosphere. Two significant modeling efforts are underway in this area of end-to-end modeling, one at the University of Michigan [*Gombosi et al.*, 2000] and the other at the Center for Integrated Space Weather Modeling [*Merkin et al.*, 2007]. However, other efforts have used empirical models of the ionospheric inputs that are driven by the observations of the Sun or solar wind to predict how the ionospheric drivers will change from a period lasting from a few hours to 24 h [*Schunk et al.*, 2004].

In contrast to these two approaches, this study focuses on a subset of ionospheric weather that is also driven by the Sun but relates to solar coronal hole fast streams, which are, in fact, very predictable [*Denton et al.*, 2009]. During the past solar minimum over approximately a 3 year period, ionospheric weather was predominantly driven by these coronal hole fast streams. This is not a unique occurrence, but due to the extended solar minimum that has provided an excellent study database. Many of these fast streams persisted for more than 6 months and some over 1 year. In section 2, the evidence to support these statements will be provided. The forecasting described does not require observational knowledge of the Sun, solar wind, or magnetosphere. Rather, it is based on the recurrence of events driven by the solar rotation period. The basic premise is that if an ionospheric weather event observed today was driven via a coronal hole, it will, with high probability, recur in one solar rotation, two solar rotations, and with decreasing fidelity in several solar rotations. Given that the solar surface is usually populated by several coronal holes located at different longitudes, their specific ionospheric impact will also be distributed through the nominal 27 day cycle. Using this recurrent feature, the ionospheric forecast scheme applied to these weather events only requires ionospheric observations, followed by the separation of the climate from the weather. Then, the weather is forecast ahead in 27 day increments and added back to the appropriate climate for that time. By making use of the unusually long recent solar minimum with long-lived coronal holes and extensive ionospheric observations, we demonstrate here how this forecast performs.

Section 2 discusses the coronal hole driver scenario, while section 3 shows how the ionospheric weather correlates to these drivers. In section 4, the ionospheric observations are separated into climatology and weather; such that in section 5, the forecast scenarios are shown and quantified. In the space weather prediction community, its ability to forecast is important for both adverse communications and satellite drag effects in the ionosphere and thermosphere, respectively [*Fedrizzi et al.*, 2012]. An operational scenario is discussed in sections 6 and 7, the discussion and conclusion sections.

2. Geospace Response to Coronal Hole Fast Streams

Space weather in geospace is typically viewed as the upper atmosphere-ionosphere-magnetosphere dynamics in response to (1) changing solar wind conditions, (2) internal plasma instabilities, and (3) changing atmospheric conditions. In this study, only type 1 of the above is considered to be the source of weather in the ionospheric observations (described in section 4.1). Two very distinct forms of solar wind dynamics exist: that generated by coronal mass ejections (CMEs) and that generated by coronal hole fast streams (CIRs). CMEs are isolated features that explode from the Sun and propagate through the heliosphere, while the CIRs are embedded features in the heliosphere associated with high speed streams (HSS) that are connected to coronal holes on the Sun. *Borovsky and Denton* [2006] listed and described these differences in detail. The most relevant difference to this study is that the CME is an isolated event, whose initiation process is not understood and hence is unpredictable. In contrast, the CIR is associated with a HSS from a coronal hole, whose life span often exceeds many solar rotations. This life span provides the possibility of a one, two, or longer solar rotation forecast (approximately 27, 54, 81, etc., day forecasts.) The understanding of how the coronal hole leads to the CIR/HSS and its subsequent impact on geospace has been widely studied and reported. For example, in the review by *Tsurutani et al.* [2006], our understanding of CIRs is described extensively. In this study, we only refer to one aspect of the solar wind CIR—namely, the time at which the slow solar wind transitions to the fast solar wind to establish an epoch time for a CIR arriving at Earth. In fact, the slow-to-fast stream transition is not a simple boundary, and various solar wind parameters are changing relatively independently over a few days as the CIR/HSS passes the Earth. From the forecast perspective, the key information can be extracted from the abstract of *Tsurutani et al.* [2006], which refers to the energy deposition in the ionosphere-thermosphere through the impact of CIRs on the auroral electroject index *AE*:

> "It is noted that the continuous *AE* activity is not a series of substorm expansion phases. Arguments are also presented why these *AE* activity intervals are not convection bays. The auroras during these continuous *AE* activity intervals are less intense than substorm auroras and are global (both dayside and nightside) in nature. Owing to the continuous nature of this activity, it is possible that there is a greater average energy input into the magnetosphere/ionosphere system during fast declining phases of the solar cycle compared with these during solar maximum."

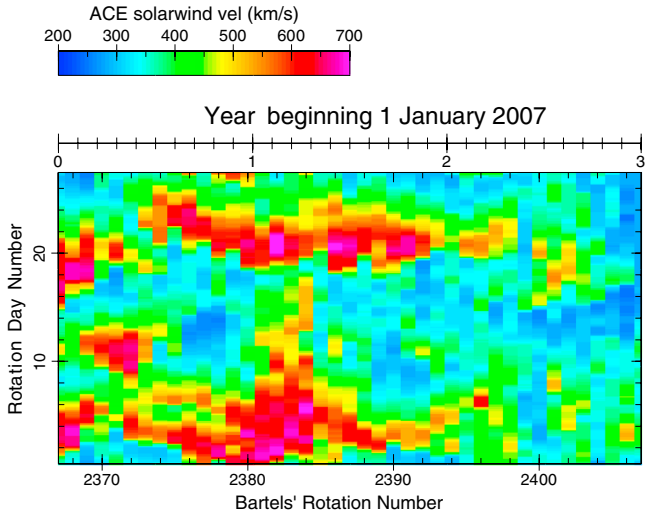

Figure 1. Binned ACE solar wind velocity organized into 27 day Bartels' Rotation Numbers and hourly within each 27 days of that rotation. The wind magnitude is color coded, and a secondary axis provides year information beginning 1 January 2007.

Thus, geospace, even during solar minimum periods, exhibits significant activity during the CIR/HSS passage, and this activity can be sustained for several days.

The NASA Advanced Composition Explorer (ACE) satellite at L1 (Lagrange point) has been used to determine when a CIR will interact with geospace [*McComas et al.*, 1998]. More recently, imagers on the two NASA STEREO satellites have been able to trace the CIR from the Sun to the Earth. This latter capability has been enabled by solar eruptions of enhanced plasma outflow at the CIR boundary. The enhanced densities produce sufficient photon scattering to exceed the sensitivity levels of the STEREO instruments, therefore making the denser CIR visible [*Rouillard et al.*, 2009, 2010a, 2010b]. Significant research has also been conducted to understand how the magnetosphere, along with its convection and energetic populations, responds to these multiday CIR events [*Denton et al.*, 2008; *Denton and Borovsky*, 2008; *Kissinger et al.*, 2010; *Borovsky and Denton*, 2010]. These studies of the magnetospheric convection and associated auroral precipitation are important for the ionosphere since they are the main ionospheric drivers during these events. How these convection and precipitation respond to a CIR/HSS still remain an outstanding question. *Kissinger et al.* [2010] show that statistically steady magnetospheric convection frequently occurs within a day of the CIR stream interface. They also found that the results of their solar minimum study differed from those of the similar studies at solar maximum.

The fact that the CIRs themselves demonstrated a well-established recurrence leads to the ability to forecast these geospace events. Discussions of how this CIR-geospace forecasting of geomagnetic indices may be implemented have been described by *McPherron and Siscoe* [2004] and *McPherron and Weygand* [2013]. For our proposed forecast scenario, it is necessary to appreciate that, indeed, CIRs do recur, and as we will show, exhibit a one-to-one correlation with an ionospheric response.

3. CIRs in the Solar Wind

The NASA ACE satellite is located near the Lagrangian point and is able to continuously monitor solar wind CIRs that will impact geospace. Studies have been carried out to describe the complex sequence of solar wind parameter variations that occur during the passage of a CIR [*Denton and Borovsky,* 2008]. Here we make use of the general CIR property that during the declining phase of the solar cycle and during solar minimum, HSSs tend to have significantly elevated ion velocities. Since the objective is to test a forecast capability, the details of the CIR are not germane at this time. Figure 1 presents the hourly ACE solar wind ion velocity in a format designed to capture a 27 day period of solar rotation using the Bartels' Rotation Number. The velocity is the median of the $\pm$12 h of ACE wind data centered on the hour in question. Each vertical color band corresponds to a sequence of 27 days, and each successive band contains the next 27 day period. A secondary horizontal axis spans the years for this data set. A study period beginning on 1 January 2007 and lasting for 3 years is shown in Figure 1. Velocities that are above 500 km/s are color coded in orange and red. These relatively large velocities represent the presence of CIR/HSS passages as detected by the ACE satellite. The most long-lived, recurrent CIR/HSS feature began at rotation 2372 and lasted until rotation 2398, a period of almost 2 years. This feature is identified as the horizontal red band between days 20 and 24 of the 27 day period. Over the same time period, a second feature occurs between days 1 and 6. However, this HSS structure is less pure with an additional solar wind activity beginning at rotation 2372 and eventually merging and fading at rotation 2384. This HSS lies at about 6 to 10 days. In the first 7 rotations, there is

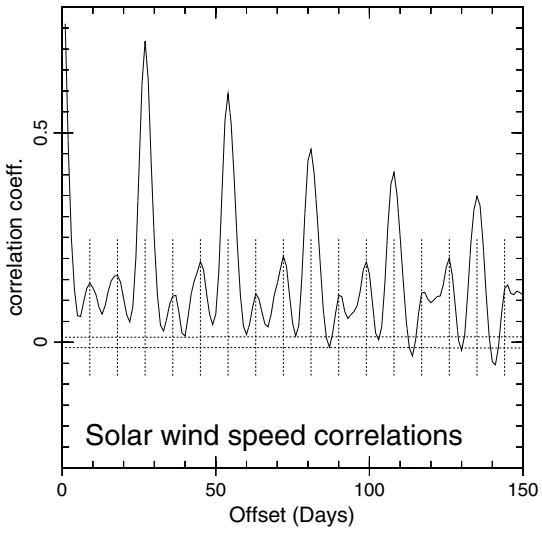

Figure 2. The 3 year solar wind ion velocity autocorrelation function for time lags that range from 1 to 150 days. Each lagged correlation computation has over 20,000 pairs of points. The dashed lines represent the standard significance bounds (95% confidence level). The vertical lines correspond to 9, 18, 27, etc., days.

an evidence for a short-lived recurrent CIR/HSS, present between days 8 and 13. In the final year shown in the figure, rotations after 2396, the Sun has reached its extremely quiescent state of the extended solar minimum between solar cycles 23 and 24. The two main CIR/HSS groups are weaker but still present.

From a visual inspection of Figure 1, the argument that one 27 day "strip" is a good representation of the next 27 day strip is not unreasonable. This leads naturally to the question of how good such a 27 day prediction would be based on today's observation. To address this quantitatively, the full 3 years of solar wind ACE ion velocity data are studied. The original ACE data used have a 1 min cadence, but for this purpose, it has been averaged over 1 h. Hence, for the 3 year interval, the sequential velocity data set has 26,304 hourly values. A second data set is needed in order to carry out a correlation calculation. The objective is to introduce offsets of 24 h (1 day) at a time, compute a correlation coefficient, then offset by a further day and repeat. This process is repeated until the two data sets are offset by 150 days. An offset of 150 days corresponds to about 5.5 solar rotations. With an offset of 24 h, the length of the two data sets is reduced from 26,304 to 26,280 because only synchronized pairs can be used. For the full 150 days, the length of the two data sets is further reduced to 19,104. Although significantly smaller, this data set is sufficient for reliable trends to be deduced. Figure 2 shows these correlation coefficients over the 150 day range of offsets. The correlation coefficient scale follows the standard convention of 1 corresponding to 100% correlation, 0 corresponding to uncorrelated, and −1 corresponding to 100% anticorrelated. The horizontal dashed lines on Figure 2 represent the standard significance bounds [*Shumway and Stoffer*, 2006]. These have been evaluated for each of the 150 correlations in Figure 2. They indicate that even the secondary correlation peaks are significant at the 95% level of correlation.

Well-defined peaks are seen in Figure 2. Dashed vertical lines have been superimposed on the figure at multiples of 9 days to aid in identifying the dates of each peak. The most strongly correlated peaks occur at days 27, 54, 81, 108, and 135 as shown by the vertical lines in the figure. These are exactly multiples of 27, the solar rotation period. However, even the secondary peaks are significant. In the first 27 days, these correspond to a peak at both 9 and 18 days. These additional enhanced correlations are also shown in Figure 2 as vertical dashed lines that are added to each subsequent 27 day lag cycle. Looking back at Figure 1, a 9 day shift will take the CIR located at about day 21 forward to day 3 of the next solar rotation. This lies on top of the other CIR, but a 9 day shift of this CIR moves it into a non-CIR region. Hence, the 9 day shift will generate a weak correlation. The same argument holds for an 18 day shift, taking the CIR at day 3 on to that at day 21. Therefore, the 27 day "forecast" concept holds at least 5 rotations into the future. The correlation coefficient at the 27 day lag is positive at a value of 0.72, and at 54 days, it has decreased to 0.58. These correlations are not 1 and is expected since the entire 3 year database shown in Figure 1 is being used. In Figure 1, there is no 27 day periodicity that extends across the entire 3 years. Significantly higher correlation coefficients would be achieved by using a shorter data set. A data set beginning at 0.5 years and extending only to 2 years of the present 3 year study (see Figure 1) would include only solar rotations with the two main CIRs.

4. Does the Ionosphere Have a 27 Day Response to the CIR?

4.1. Poker Flat Incoherent Scatter Radar

The National Science Foundation (NSF) Poker Flat Incoherent Scatter Radar (PFISR) located at the Poker Flat Research Range in Fairbanks, Alaska (65.13°N, 147.47°W), began its 24/7 operations on 1 March 2007. This

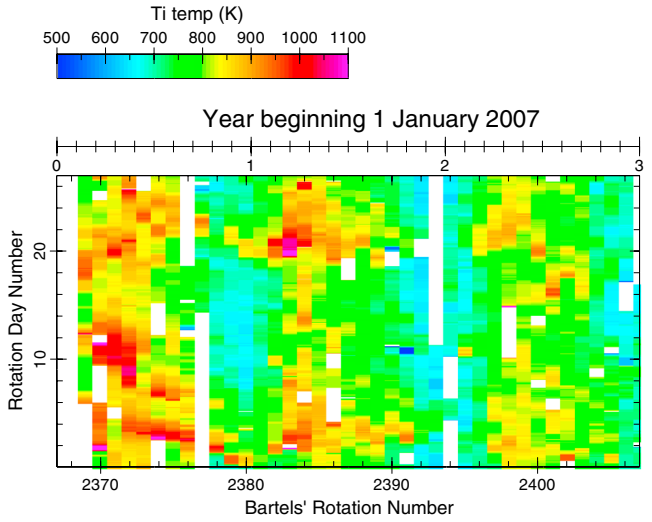

Figure 3. Binned PFISR ion temperature at 300 km organized into 27 day Bartels' Rotation Numbers and hourly within each 27 days of that rotation. The temperature is color coded, and a secondary axis provides year information. White areas on this plot represent periods of no PFISR observations or when the median value was less than 500 K. Note that regular PFISR operations began on 1 March 2007.

coincided with the beginning of the International Polar Year (IPY). PFISR has been running continually in this mode, interrupted only for specific scientific campaigns, support of Poker Flat rocket launches, and technical issues/maintenance. Of unique relevance is that PFISR measurements are plasma density and ion and electron temperature profiles taken at a cadence of 10–15 min. There is no other technique that can capture these complete plasma profiles through the E and F layers of the ionosphere. Furthermore, an extension to this 24/7 mode was the addition of Doppler ion velocity measurements from multiple look directions, which enable electric fields to be inferred [*Heinselman and Nicolls*, 2008]. The experimental mode for the IPY and beyond had been described by *Sojka et al.* [2009a]. For this study, ion temperatures from a field-aligned look direction will be used to demonstrate that, indeed, the auroral as well as the dayside midlatitude ionosphere respond to every CIR that impacts geospace, and as a consequence, provides the basis for long-range ionospheric weather forecasts during the declining phase of the solar cycle.

Figure 3 is in the same format as Figure 1 and represents the hourly median over a centered 24 hour interval of ion temperature at 300 km as observed by PFISR. This parameter at this altitude has been chosen since it has a rapid response to magnetospheric energy input, and at this altitude, tracks the thermospheric exospheric temperature under quiescent conditions [e.g., *Conde and Nicolls*, 2010]. The ion temperature at 300 km in Figure 3 does not mimic the solar wind velocity but does show similarities. The uncolored areas (white) in Figure 3 represent the periods of at least 1 day when no PFISR measurements were available or when the median ion temperature fell below the 500 K lower threshold. This multiyear data set is also sensitive to seasonal and diurnal variations, the dependence being quite independent of the solar wind, its velocity, or other parameters. During this extended solar minimum period of almost 3 years, the seasonal and diurnal ionization source, the solar EUV flux, was almost constant. This unique condition along with the almost continuous diurnal and seasonal PFISR measurements enable the background ion temperature climate to be extracted.

4.2. The Background Ion Temperature at 300 km

In an earlier study, *Sojka et al.* [2009a] showed examples of how the ion temperature history could be separated into active and quiescent days, with the former associated with elevated ion temperatures. This knowledge is used to select the coldest ion temperature every half hour of universal time within each 27 day period. By repeating this process for fourteen 27 day periods the annual season (14 bins) and local time (48 bins) climatology was obtained. Figure 4 shows this cold Ti climatology over 1 year of the IPY observational program. In this figure, the ionospheric seasons are evolving from spring equinox for the first solar rotation and proceed to reach summer conditions about 100 days later; then the winter season was encountered about a further 200 days later. Thus, neither the observational 27 day solar rotations nor the calendar days are readily correlated to season. Hence, a simple day count has been used to organize the 27 day solar rotation coldest Ti values during the UT day. The summer maximum in ion temperature is evident around day 100, while a cold winter minimum is observed around day 300. The diurnal variation associated with the local time of Poker Flat is very evident. Local noon occurs at about 2200 UT, while midnight is around 1000 UT. In summer, Poker Flat is sunlit all day with elevated temperatures, whereas in the winter it is dark all day and as a result the ion temperatures are colder. The dynamic range for both seasonal and diurnal variations are almost a factor of 2, ranging from almost as low as 500 K to just

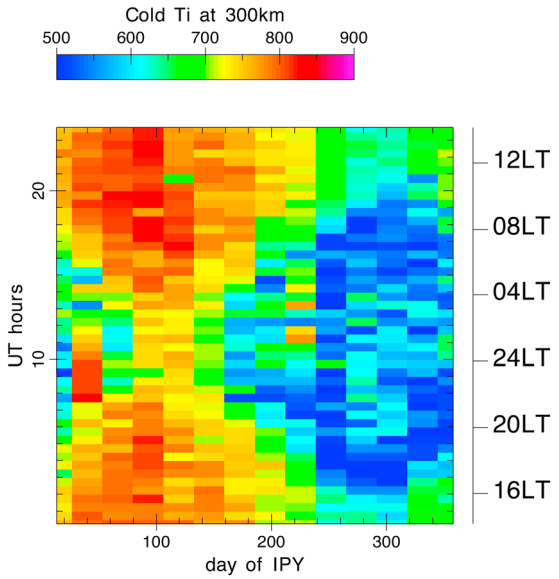

Figure 4. The PFISR coldest temperatures at 300 km during the entire IPY binned into 27 day solar rotations and half-hour UT bins. The ion temperature is color coded, and no smoothing has been applied. A PFISR solar local time hour axis is shown at the right of the panel. The IPY day number is a sequential day sequence beginning on 1 March 2007.

over 800 K. Note in Figure 4, no smoothing or rejection of data has occurred, and some of the half-hour UT bins appear to be anomalous. For example, day 40, between 0700 and 1100 UT, and day 220, between 1000 and 1400 UT, appear anomalous. These anomalies correspond to 27 day intervals, where data gaps and quiet conditions coincide resulting in rather warmer "lowest temperatures." Unlike the situation of data gaps in Figure 3, the absence of data on a quiet day during a 27 day solar rotation period means that the cold Ti is taken from another day. Therefore, there are no missing bins in this format; rather, the procedure may not always capture the coldest temperature for that half-hour UT and solar rotation. Figure 4 is unique in its own right since ion temperature measurements are difficult to make and data sets over the entire seasons and local time cycles are rare. This type of data will provide the broader IRI and empirical modeling community with a valuable validation data set.

4.3. Residual Enhanced Ion Temperature at 300 km

Using the background cold temperature climatology as a reference, a residual elevated ion temperature can be determined. A bicubic spline interpolation applied to the cold temperature distribution shown in Figure 4 was used to interpolate to a specific day of year and UT. Each individual temperature measurement was subsequently referenced to this cold temperature, and a residual enhancement was determined. Figure 5 is in the same format as Figure 3 and shows these residual temperatures. The uncolored areas (white) in Figure 5 represent periods of at least 1 day when no PFISR measurements were made. This residual ion temperature distribution is significantly closer in morphology with the solar wind velocity, shown in Figure 1. Beyond rotation 2385 (1.5 year mark), which corresponds to about summer of 2008, both the strength of the solar wind HSS velocities and the enhanced ion temperatures begin to decrease. However, they still appear correlated in the days on which they occur. Figure 5 shows that from one 27 day rotation to the next, there is almost always a strong similarity in the 27 day variation. This is the crux of a 27 day ionospheric weather forecast. After removing the diurnal and seasonal variations, the dominant ionospheric dependence lies with the 27 day solar rotation. It is noted that the last few solar rotations at the close of the third year show elevated ion temperatures. These enhancements do not correlate with solar wind CIR-type enhancements in Figure 1.

A lagged correlation analysis was carried out on the residual ion temperatures shown in Figure 5. Daily lags of up to 150 days similar to the earlier ACE solar wind analysis were used. The ion temperature residuals were first binned into hourly averages. Two synchronized sequences, the daily lagged and unlagged time series, were obtained. However, data gaps exist in both sequences. Therefore, a search was made for hourly data gaps and for each of the data sets the corresponding hourly values were removed. This reduces the length of the sequences by one for each hourly data gap. Even so, the sequences had more than 20,000 hourly values available. As can be seen in Figure 3 and again in Figure 5, entire days were often missing and almost a whole month at rotations 2376–2377 (0.75 years). This missing month corresponds to the time when PFISR was upgraded to complete the antenna face.

The correlation study was carried out on the ion temperature residuals. Figure 6 shows the results of the correlation analysis with the standard (95%) significance bounds shown by the dashed lines. Evident in the Ti residual correlation is a repeating pattern that has strong correlations at the 27 day period and two secondary correlation peaks between the strong correlations. This pattern matches in that shown in Figure 2 for the solar wind velocity correlation. Vertical dashed lines indicate the sequence of days 9, 18, and 27 repeated over

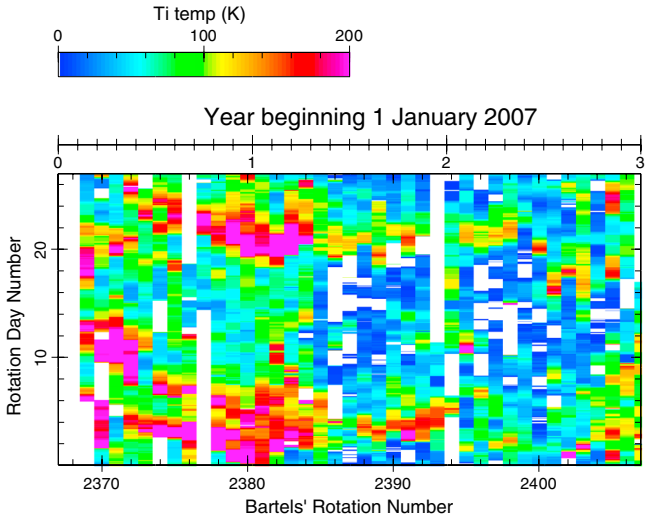

Figure 5. The hourly median from a centered 24 h interval of the residual PFISR ion temperature at 300 km altitude. The ion temperature is color coded and plotted in 27 day vertical strips. The solar rotation and year formats are the same as for Figure 3. White areas on this plot represent periods of no PFISR observations. Note that regular PFISR operations began on 1 March 2007.

the entire 150 day lag study. These days are the same as shown in Figure 2 and as in Figure 2 line up with both the primary and secondary peaks in the correlations. The peak magnitudes are somewhat less in the ion temperature case. However, this correlation provides the basis for a forecast capability that extends in the cycles of 27 days.

4.4. Local Time Correlations and Short-Duration Heating Mitigation

Two additional dependences exist in the Ti data at 300 km that impact the correlations seen in section 4.3. These can be accounted for, and as a result, provide a more refined forecast capability. The local time dependence pertains to the fact that the Poker Flat location is not always in the same geomagnetic region. Around local noon, PFISR is located well equatorward of the cusp, and hence, it is a midlatitude location. For very quiet geomagnetic conditions in the midnight sector, this location can be colocated with the midlatitude trough. Therefore, it would seem possible that the section 4.3 correlation study may have a local time dependence or there could be local times such as around midnight when trough *F* region densities become very small, leading to larger standard errors in the observations. In order to test this scenario of local time dependence, the ion temperature data set was subdivided into six, 4 h LT data sets. For each of these six data series, there are up to 4 hourly values each day within their local time interval. But to minimize the effect of data gaps, these 4 bins are averaged to give a simple value each day. Hence, from a correlation perspective, instead of 16,000 hourly values, there are now only a maximum of 1096 values. In fact, because of PFISR off-line periods or other campaign modes, the number of days is closer to 800.

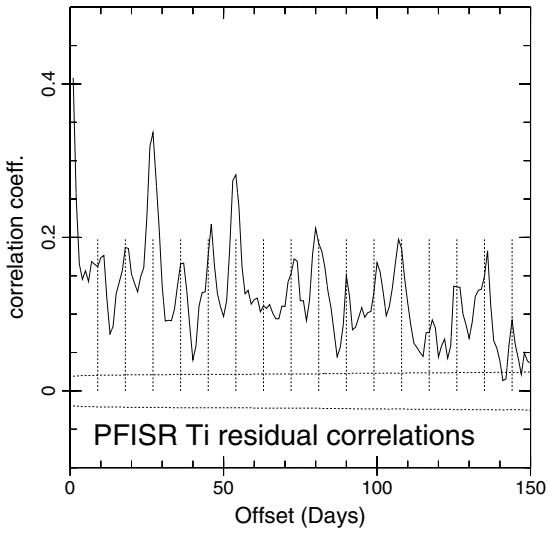

Figure 6. Three-year PFISR, residual ion temperature autocorrelation function for time lags ranging from 1 to 150 days. The lagged correlations have between 6000 and 10,000 pairs of hourly points. The horizontal dashed line represents the standard (95%) significance bounds. The vertical lines correspond to 9, 18, 27, etc., days.

The second issue pertains to the dual character of the ion temperature heating during HSS. In earlier studies [*Sojka et al.,* 2009a, 2009b], examples of the CIR signature in Ti showed that over a period of 1 to 3 days, the ion temperature was enhanced by up to 200 K. This is consistent with the daily average residual temperatures shown in Figure 5. However, superimposed upon this are bursts of much larger heating. These bursts had durations of tens of minutes to an hour. Note that in Figure 5, which consists of daily averaged Ti residual values, these bursts were not removed but have somewhat enhanced the daily average. The burst probably represents local ion-frictional heating during electric field enhancements associated with substorm-type main phases. In this study, it is the former 200 K overall heating that is viewed as being able to be forecast, not the individual heating bursts.

A method of removing these bursts was developed using 4 h LT binning to determine if a

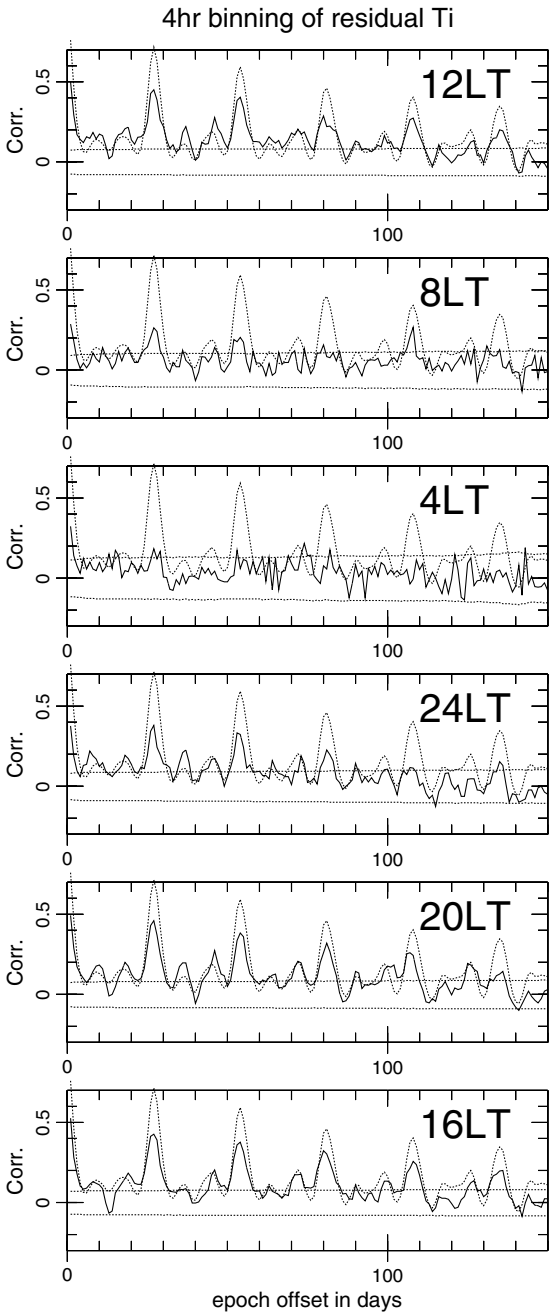

Figure 7. Residual Ti lagged correlation analysis for PFISR residual binned into 6 local time bins. Each panel identifies the Poker Flat local time at the center of each bin. The dashed line repeats the ACE solar wind velocity correlation shown in Figure 2. The horizontal lines shown the 95% significance levels for each local time bin.

local time dependence could be found. Each 4 h data set could have a maximum of 24, 10 min ion temperature values. A typical heating burst would last up to an hour; hence, up to 6 of these 24 values would be extensively heated. Therefore, a selection was made from the 24 values; specifically, the middle two quartiles were used to compute a revised 4 h local time average ion temperature. Note that not all of the 4 h intervals have 24 ion temperature measurements; in such a case, the algorithm requires at least eight samples to infer an average.

The six panels of Figure 7 show the individual local time ion temperature correlations, along with 95% significance lines for each local time period. Superimposed upon each panel is the Figure 2 solar wind correlation as a dashed line. The panels indicate that the ion temperature and solar wind velocity CIR correlations vary as a function of local time. Indeed, some of the panels show correlations that are stronger than those for the full ion temperature data set shown in Figure 6. The least correlated at the 27 day period is found in the 4 and 8 LT sectors. In the 4 LT panel, no correlation is obtained at the 95% confidence level, while in the 8 LT panel, the correlations at 27, 54, and 108 day lags exceed the 95% confidence threshold. Over a year, this local time sector will have the lowest electron density, which potentially creates significant statistical issues. Four of the local time panels: 12, 16, 20, and 24 h show very good agreement with the correlation results from the ACE solar wind velocity (dashed line) of Figure 2. The agreement occurs not only at 27 days but also through at least 3 solar rotations. The presence of weaker correlations between the 27 day multiples also exhibits similarities with the solar wind velocity. For subsequent study, the 16 LT local time data will be used.

5. The 27 Day Forecasting of the Ion Temperature

Historically, the high-latitude ionosphere has been viewed as a region subject to storms and substorms that produce weather, but the cadence or even duration of that weather cannot be forecasted. Most schemes that attempt to forecast the ionosphere are based on climatology or on detected changes in the Sun or solar wind that will propagate to geospace and lead to storm-type weather [*McPherron and Weygand,* 2013; *Schunk et al.*, 2005]. This study, in contrast, has concentrated upon a phenomenon that is caused by the Sun, coronal hole fast streams, and lasts for many solar rotations. Once such an HSS creates a CIR that impacts geospace, a corresponding ionospheric response is observed. Each such CIR/HSS then reappears 27 days later, and usually, continues to reappear for many rotations, as demonstrated in Figures 5, 6, and 7. This 27 day recurrence of enhanced residual ion temperature is shown to

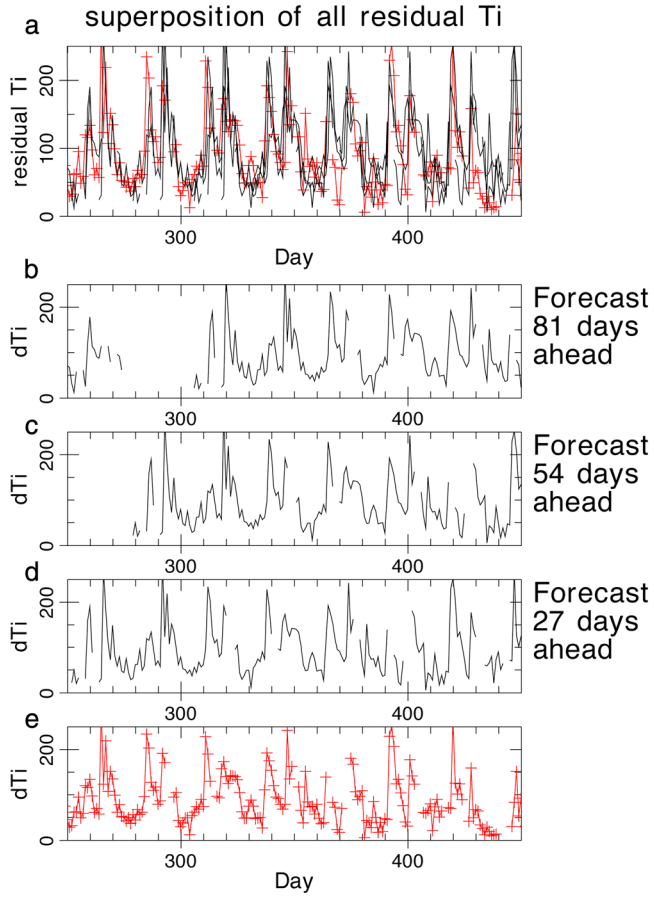

Figure 8. (a) Superimposition of all the four data sets. (b–d) The time series shifted in time by 27, 54, and 81 days. (e) The PFISR 1400 to 1800 LT residual temperature over 200 days, beginning on day 250. A superimposition of Figures 8b–8e is shown in Figure 8a. In both Figure 8a and 8e, the original residual temperature data is shown by red plus symbols and connected with red lines.

be very predictable. By examining the narrowness of the correlation spike at 27 days in Figure 6 and some panels of Figure 7, one finds that the prediction recurrence has only a $\pm$1 day uncertainty. This occurs even though a typical CIR/HSS itself has a duration of several days. However, the CIR/HSS duration is not a symmetric event; rather, it has a rapid rise and a slow decay [*Sojka et al.*, 2009b]. As a first step in forecasting 27 days in advance, one needs only the current ionospheric ion temperature. By removing the appropriate seasonal and diurnal variation, as shown in Figure 4, a residual ion temperature is obtained. This can then be projected 27, 54, and even 81 days ahead to form the basis of a residual Ti forecast. Then, the seasonal and diurnal climate at 27, 54, or 81 days can be added to this forecast residual to create the full Ti forecast. In this first application of 27 day forecasting, no attention has been paid to how the CIR/HSS is evolving over many solar rotations. Figures 2 and 6 both indicate that as the forecast period increases, the degree of correlation diminishes. This information has not been incorporated into the present forecast scheme.

Figure 8 shows a reconstruction of the Ti residuals from day 250 (7 September 2007) through day 450 (25 March 2008). Figure 8e is the average PFISR Ti residual (red + symbols) over 1400–1800 LT, with ion temperature bursts removed as described previously. Figures 8b–8d corresponds to a 27, 54, and 81 forecast for these 200 days, using the appropriate prior Ti residuals. Figure 8a is a superimposition of all the four data sets, with the red trace corresponding again to the PFISR Ti residual. Figure 8a provides ample visual evidence for how systematic the ionospheric response is to this series of 7 solar rotations. A more quantitative measure is found by differencing each forecast from the truth (Figure 8e). This generates a distribution of differences centered near zero kelvin with a variance that ranges between 20 and 50 K. However, over the 200 days, no systematic recurrence of a 27 day oscillation persists in this difference. This variance itself is relatively small compared to the forecast events that are greater than 100 K often extending over 200 K. Each of the 7 rotations has two very identifiable Ti peaks. These correspond to the two vertical bands seen in Figure 5 and in the solar wind velocity of Figure 1. Figure 8e shows the 4 h average values from the 1400 to 1800 LT section. This data set has only one value per day and there are data gaps. Indeed, from this time series alone, it is not possible to infer the strong recurrence of heating events seen in Figure 8a.

The seasonal climate variation between 1400 to 1800 local time is shown in Figure 9 (bottom) as a dashed line along with the measured ion temperature at 300 km. This plot is centered around winter solstice (day 355), when the temperature climate contributions are low and spans the same time period as in Figure 8e. In this example, the residual ion temperature contribution reaches almost 40% of the expected seasonal climate temperature. Figure 9 (top) is the reconstruction of the 27, 54, and 81 day prediction for the ion temperature

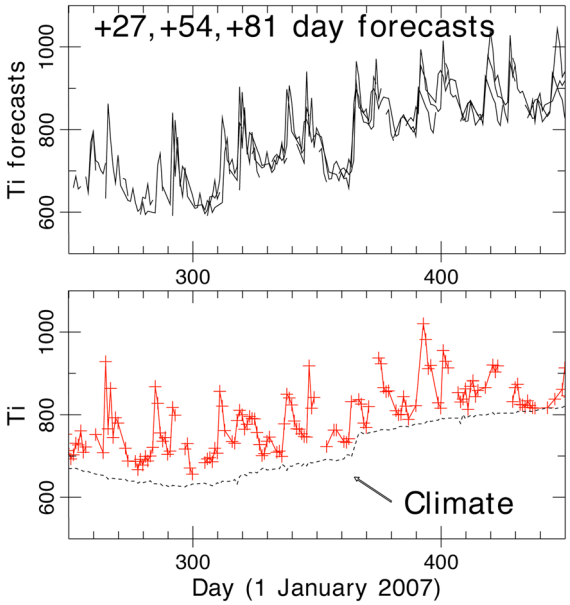

Figure 9. (top) The three forecasts of the ion temperature: 27, 54, and 81 days. (bottom) PFISR, 1400 to 1800 LT, Ti at 300 km (line) and PFISR cold climate (dashed line) between days 250 and 450.

at 300 km above Poker Flat. The prediction adds the forecasted residual ion temperatures of Figure 8 to the appropriate climate value.

In Figures 8 and 9, the forecast has been made during favorable conditions; i.e., winter season, where the contrast between residual heating and background temperature is largest, and also during a long period of strong and stable coronal holes on the Sun. In Figure 1, the CIR/HSS strengths begin to diminish after the middle of the second year, and summer conditions are experienced. The prediction analysis has been repeated for this period, days 450 to 650, and is shown in Figure 10. Although the residual Ti heating events are significantly weaker, the long-term 27, 54, and 81 day forecasts are still well correlated with the observations.

6. Discussion

6.1. Upper Atmospheric and Ionospheric Inputs

Over a 3 year period, this study has shown that ion heating events in the auroral ionosphere over Poker Flat have an inherently predictable character. Although this study has focused on one ionospheric parameter, the ion temperature, at a single altitude and location, is representative of a much broader predictable impact. Even beyond these ionospheric parameters, the recurrence of events in other ionospheric and thermospheric parameters has been found.

In each case, the physical processes leading to both the ionosphere and thermosphere (IT) response to HSSs are associated with magnetospheric energy deposition in the IT and the subsequent redistribution of this energy within the thermosphere. Thermospheric studies have shown that the neutral density has 7 and 9 day periodic variations that were highly correlated with CIRs [*Lei et al.*, 2008a, 2008c; *Thayer et al.*, 2008]. *Chang et al.* [2009] showed that such a correlation existed at altitudes as low as 110 km in the neutral temperature, and *Crowley et al.* [2008] found that the correlation existed for the neutral composition. Ionospheric total electron content correlations were also found [*Lei et al.*, 2008b; *Pedatella et al.*, 2010] and in N_mF_2 and by in situ satellite measurements of the electron density [*Denton et al.*, 2009; *Pedatella et al.*, 2010]. *Sojka et al.* [2009b] found that at high latitudes, the ion temperature at 300 km also showed this CIR correlation.

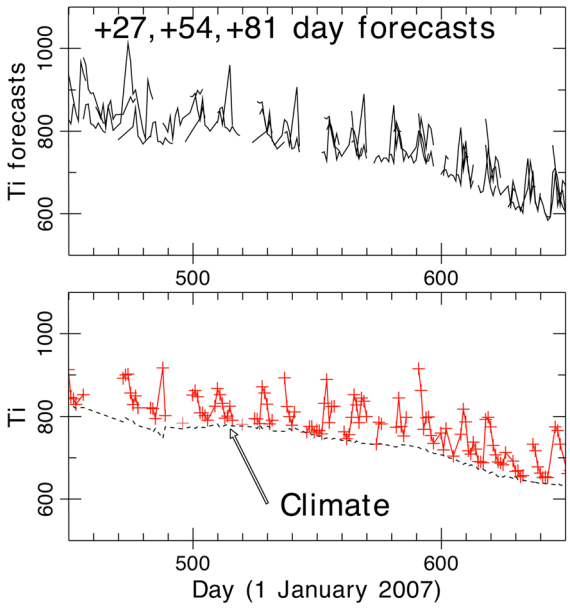

Figure 10. Same PFISR forecast as in Figure 9 but for the period of days 450 to 650.

Heelis and Sojka [2011] used DMSP satellite plasma drift measurements to demonstrate that during CIR events, the high-latitude plasma drifts are enhanced. The enhancements are consistent with the

magnetospheric electric field being enhanced. During these periods, the region being directly influenced by the CIR expands equatorward into the midlatitudes. In the ionosphere, the ion friction heating mechanism rapidly produces ion temperature increases, the parameter identified in this study. Other parameters specifically the plasma density, plasma velocity, and electron temperatures all show CIR response at the *F* peak and through to the topside. However, additional physical processes modify the direct CIR influence on these parameters. Figures 3, 4, and 5 provide a measure of how the IPY period CIR changed the *F* region ion temperature over the climatological background. The climatological temperature range was from 500 to 900 K (Figure 4) depending on season and local time, while the stronger PFISR CIR events produced 100 to 250 K (Figure 5) ion temperature enhancements. Unlike a short-lived substorm heating event (typically 3 h), the CIR heating last over a day. Hence, the CIR ion heating is readily identified and probably not as locally confined as a substorm energy deposition. There is a need to better understand the evolution of the magnetospheric electric field and its associated precipitation characteristics during a CIR. With such knowledge, present-day physics-based models of the ionosphere and thermosphere would probably be able to describe the overall impact of CIR in the IT.

6.2. Operational Forecast Scenario

Forecasting upper atmospheric density and ionospheric changes are tasks of interest for tracking satellites and for radio communications in the polar regions, especially under emergency conditions. The scientific understanding of how well the upper atmosphere or ionosphere is able to be forecasted falls well short of operational needs. A reasonable present-day forecast scenario is based upon the NASA space assets such as the new SDO satellite, with the STEREO satellite observing the launch of a coronal mass ejection that is deemed to impact geospace and likely to create a geomagnetic storm. This scenario can provide a 1–2 day forecast. The next step in validating the forecast is for the NASA ACE satellite located at L1 to respond to the CME arrival and determine the CME polarity, which enables the estimates of the magnitude of the ensuing geomagnetic storm. At present, there is a 30 to 60 min warning of the impending geomagnetic storm. These CME-generated geomagnetic storms represent the most intense space weather events in the upper atmosphere and ionosphere. However, they are only forecastable with a 1–2 day lead time.

A second level of geomagnetic storm associated with the CIR/HSS events is described in this research. Although this study has focused on an extended 3 year solar minimum interval, these CIRs occur throughout the solar cycle. During solar minimum, the presence of large CMEs is almost nonexistent, enabling this study to clearly demonstrate the repeatability and the predictability of the CIR-generated geomagnetic storms. Although devoid of CMEs, the solar minimum CIR generates relatively weaker geomagnetic storms than CIRs occurring during more active phases of the Sun.

In this study a key step was the identification of quiet periods such that the seasonal and diurnal morphology of the ion temperatures observed by PFISR would be made. Using this morphology, Figure 4 was possible to remove both the seasonal and diurnal dependence from the PFISR observations and hence transform Figure 3 into Figure 5. This procedure would likely be more challenging if applied to higher levels of solar activity. During such conditions, the space weather levels of activity are enhanced, and finding 2 or 3 day sequences of quiet conditions is more difficult then at solar minimum. A future study is needed to quantify this procedure to obtain the seasonal and diurnal morphology. Fortunately, PFISR has been making the measurements through the recent solar maximum period to enable this study.

With the caveats of this solar minimum study in mind, it is possible to consider how CIR/HSS-generated geomagnetic storms at higher points in the solar cycle might be operationally forecast at least 1 solar rotation into the future. The identification of solar coronal holes, the source of the CIRs, is well understood and routinely carried out from solar observations. However, not all coronal holes lie at geoeffective solar latitudes. As coronal holes migrate from high solar latitudes toward the solar equator, their solar wind fast streams can flow across geospace at certain latitudes and hence become geoeffective. With a satellite located at L1, such as the NASA ACE satellite, a direct measure of the effectiveness of the CIR is made. However, as stated earlier, this provides less than 60 min of warning. As a result, the forecast procedure relies on identifying this CIR as geoeffective. The forecast is that 27 days ahead there is a high probability that this CIR will reappear. During solar maximum, the recurrence of a specific coronal hole is known to last for only a few solar rotations; this is in contrast to our study in solar minimum, where two coronal hole regions remained geoeffective for over a year. However, even one recurrence provides a basis for a forecast.

Operationally, a number of caveats still need to be understood in order to provide quantitative estimates of the forecasted CIR geomagnetic storm. These include the following:

1. Although coronal holes are associated with HSS, the intersection of the HSS with the Earth causing a geospace event depends in part of the location on the coronal hole on the solar disk. Hence, as the coronal hole migrates equatorward on the solar disk, knowing when its HSS interacts with the Earth, is an outstanding question.
2. It is not well understood how the magnitude of each CIR-driven geomagnetic storm is related to L1 or solar observations.

As a result of these and other considerations, at the present time, an operational forecast would tend to be a qualitative statement that in 27 days from this CIR, a similar 3 day disturbance of the high-latitude upper atmosphere and ionosphere will occur with high probability. This forecast defines specific 3 day periods in the future when operations associated with satellite drag and emergency radio communications could be affected. Operationally, the major impact is expected in polar-auroral regions, a region where emergency radio communications is of concern for transpolar flights.

7. Conclusion

The ionospheric ion temperature observed at 300 km above Poker Flat, Alaska, by PFISR has produced the following conclusions for the solar minimum period studied:

1. The ion temperature residuals are correlated with solar wind velocity due to recurrent CIR/HSS events, as demonstrated by comparing Figures 2 and 6.
2. The ion temperature residuals are all heating events with temperature increases in the background ranging up to 200 K and sustained for several days.
3. These heating events can be forecasted over many solar rotations; Figures 9 and 10 demonstrate forecasts for up to 4 solar rotations (108 days).

An operational forecast scenario is discussed, based upon present-day resources. Namely, solar observations together with L1 monitoring of the solar wind can establish the presence of a geoeffective coronal hole/CIR. The forecast is then that in 27 days, there is a high probability that this same CIR/HSS will generate a geomagnetic storm. The caveats are that during solar minimum, these geomagnetic responses are weak but recur frequently, while at solar maximum, the geomagnetic response is significant, but their recurrence may only last for a few solar rotations.

At this time, the forecasts are specific in time. The details of the full ionospheric response require better knowledge of the full geospace response to CIRs. Future work on observing the convection and precipitation during CIR events will define the energy transfer function into the IT system.

Acknowledgments
This research was supported by NSF grant ATM-0408592 and AGS-0962544 to USU. PFISR is operated by SRI International under NSF cooperative agreement AGS-1133009. The solar wind CIR data were obtained from the ACE and WIND satellites. The PFISR observations used in this study are publically available from the Madrigal data archive at http://isr.sri.com/madrigal/. The International Space Science Institute is gratefully acknowledged for its role in sponsoring the IPY team meetings on this research topic.

References

Araujo-Pradere, E. A., T. J. Fuller-Rowell, M. V. Codrescu, and A. Anghel (2004), Evaluation and prospects for storm-time corrections in the International Reference Ionosphere, *Adv. Space Res.*, *33*, 902–909, doi:10.1016/j.asr.2003.07.10.

Bilitza, D. (2001), International Reference Ionosphere 2000, *Radio Sci.*, *36*(2), 261–275.

Borovsky, J. E., and M. H. Denton (2006), Differences between CME-driven storms and CIR-driven storms, *J. Geophys. Res.*, *111*, A07S08, doi:10.1029/2005JA011447.

Borovsky, J. E., and M. H. Denton (2010), Magnetic field at geosynchronous orbit during high-speed stream-driven storms: Connections to the solar wind, the plasma sheet, and the outer electron radiation belt, *J. Geophys. Res.*, *115*, A08217, doi:10.1029/2009JA015116.

Chang, L. C., J. P. Thayer, J. Lei, and S. E. Palo (2009), Isolation of the global MLT thermal response to recurrent geomagnetic activity, *Geophys. Res. Lett.*, *36*, L15813, doi:10.1029/2009GL039305.

Conde, M. G., and M. J. Nicolls (2010), Thermospheric temperatures above Poker Flat, Alaska, during the stratospheric warming event of January and February 2009, *J. Geophys. Res.*, *115*, D00N05, doi:10.1029/2010JD014280.

Crowley, G., A. Reynolds, J. P. Thayer, J. Lei, L. J. Paxton, A. B. Christensen, Y. Zhang, R. R. Meier, and D. J. Strickland (2008), Periodic modulations in thermospheric composition by solar wind high speed streams, *Geophy. Res. Lett.*, *35*, L21106, doi:10.1029/2008GL035745.

Denton, M. H., and J. E. Borovsky (2008), Superposed epoch analysis of high-speed-stream effects at geosynchronous orbit: Hot plasma, cold plasma, and the solar wind, *J. Geophys. Res.*, *113*, A07216, doi:10.1029/2007JA012998.

Denton, M. H., J. E. Borovsky, R. B. Horne, R. L. McPherson, S. K. Morley, and B. T. Tsurutani (2008), High-speed solar wind streams: A call for key research, *Eos Trans. AGU*, *89*(7), 62, doi:10.1029/2008EO070002.

Denton, M. H., T. Ulich, and E. Turanen (2009), Modification of mid-latitude ionospheric parameters in the F2 layer by persistent high-speed solar wind streams, *Space Weather*, *7*, S04006, doi:10.1029/2008SW000443.

Fedrizzi, M., T. J. Fuller-Rowell, and M. V. Codrescu (2012), Global Joule heating index derived from thermospheric density physics-based modeling and observations, *Space Weather*, *10*, S03001, doi:10.1029/2011SW000724.

Gombosi, T. I., et al. (2000), Multiscale MHD simulation of a coronal mass ejection and its interaction with the magnetosphere-ionosphere system, *J. Atmos. Sol. Terr. Phys.*, *62*(16), 1515–1525, doi:10.1016/S1364-6826(00)00091-2.

Heelis, R. A., and J. J. Sojka (2011), Response of the topside ionosphere to high-speed wind streams, *J. Geophys. Res.*, *116*, A11314, doi:10.1029/2011JA016739.

Heinselman, C. J., and M. J. Nicolls (2008), A Bayesian approach to electric field and E-region neutral wind estimation with the Poker Flat Advanced Modular Incoherent Scatter Radar, *Radio Sci.*, *43*, RS5013, doi:10.1029/2007RS003805.

Kissinger, J., R. L. McPherron, V. Angelopoulos, T.-S. Hsu, and J. P. McFadden (2010), An investigation of the association between steady magnetospheric convection and CIR stream interfaces, *Geophys. Res. Lett.*, *37*, L04105, doi:10.1029/2009GL041541.

Lei, J., J. P. Thayer, J. M. Forbes, E. K. Sutton, and R. S. Nerem (2008a), Rotating solar coronal holes and periodic modulations of the upper atmosphere, *Geophys. Res. Lett.*, *35*, L10109, doi:10.1029/2008GL033875.

Lei, J., J. P. Thayer, J. M. Forbes, Q. Wu, C. She, W. Wan, and W. Wang (2008b), Ionosphere response to solar wind high-speed streams, *Geophys. Res. Lett.*, *35*, L19105, doi:10.1029/2008GL035208.

Lei, J., J. P. Thayer, J. M. Forbes, E. K. Sutton, R. S. Nerem, M. Temmer, and A. M. Veronig (2008c), Global thermospheric density variations caused by high-speed solar wind streams during the declining phase of solar cycle 23, *J. Geophys. Res.*, *113*, A11303, doi:10.1029/2008JA013433.

McComas, D. J., S. J. Bame, P. Barker, W. C. Feldman, J. L. Phillips, P. Riley, and J. W. Griffee (1998), Solar wind electron proton alpha monitor (SWEPAM) for the Advanced Composition Explorer, *Space Sci. Rev.*, *86*(1/4), 563–612.

McPherron, R. L., and G. Siscoe (2004), Probabilistic forecasting of geomagnetic indices using solar wind air mass analysis, *Space Weather*, *2*, S01001, doi:10.1029/2003SW000003.

McPherron, R. L., and J. Weygand (2013), The solar wind and geomagnetic activity as a function of time relative to corotating interaction regions, in *Recurrent Magnetic Storms: Corotating Solar Wind Streams*, *Geophys. Monogr. Ser.*, vol. 167, edited by B. Tsurutani, pp. 125–137, AGU, Washington, D. C., doi:10.1029/167GM12.

Merkin, V. G., M. J. Owens, H. E. Spence, W. J. Hughes, and J. M. Quinn (2007), Predicting magnetospheric dynamics with a coupled Sun-to-Earth model: Challenges and first results, *Space Weather, 5*, S12001, doi:10.1029/2007SW000335.

Pedatella, N. M., J. Lei, J. P. Thayer, and J. M. Forbes (2010), Ionosphere response to recurrent geomagnetic activity: Local time dependency, *J. Geophys. Res.*, *115*, A02301, doi:10.1029/2009JA014712.

Rouillard, A. P., et al. (2009), A multispacecraft analysis of a small-scale transient entrained by solar wind streams, *Solar Phys.*, *256*, 3007–326, doi:10.1007/s11207-009-9329-6.

Rouillard, A. P., et al. (2010a), Intermittent release of transients in the slow solar wind: 1. Remote sensing observations, *J. Geophys. Res.*, *115*, A04103, doi:10.1029/2009JA014471.

Rouillard, A. P., et al. (2010b), Intermittent release in the slow solar wind: 2. In situ evidence, *J. Geophys. Res.*, *115*, A04104, doi:10.1029/2009JA014472.

Schunk, R. W., et al. (2004), Global assimilation of ionospheric measurements (GAIM), *Radio Sci.*, *39*, RS1S02, doi:10.1029/2002RS002794.

Schunk, R. W., L. Scherliess, J. J. Sojka, D. C. Thompson, and L. Zhu (2005), Ionospheric weather forecasting on the horizon, *Space Weather*, *3*, S08007, doi:10.1029/2004SW000138.

Shumway, R. H., and D. S. Stoffer (2006), *Time Series Analysis and its Applications With R Examples*, 2nd ed., edited by G. Casella, S. Fienberg, and I. Olkin, Springer, New York City, N. Y.

Sojka, J., M. J. Nicolls, C. J. Heinselman, and J. D. Kelly (2009a), The PFISR IPY observations of ionospheric climate and weather, *J. Atmos. Sol. Terr. Phys.*, *71*, 771–785, doi:10.1016/j.jastp.2009.01.001.

Sojka, J., R. L. McPherron, A. P. van Eyken, M. J. Nicolls, C. J. Heinselman, and J. D. Kelly (2009b), Observations of ionospheric heating during the passage of solar coronal hole fast streams, *Geophys. Res. Lett.*, *36*, L19105, doi:10.1029/2009GL039064.

Sojka, J. J., R. W. Schunk, M. D. Bowline, J. Chen, S. Slinker, J. Fedder, and P. J. Sultan (1998), Ionospheric storm simulations driven by magnetospheric MHD and by empirical models; with data comparisons, *J. Geophys. Res.*, *103*, 20,669–20,684, doi:10.1029/998JA01744.

Thayer, J. P., J. Lei, J. M. Forbes, E. K. Sutton, and R. S. Nerem (2008), Thermospheric density oscillations due to periodic solar wind high-speed streams, *J. Geophys. Res.*, *113*, A06307, doi:10.1029/2008JA013190.

Tsurutani, B. T., et al. (2006), Corotating solar wind streams and recurrent geomagnetic activity: A review, *J. Geophys. Res.*, *111*, A07S01, doi:10.1029/2005JA011273.